Advanced Materials Research - Details

ISSN: 1662-8985

About:

"Advanced Materials Research" is a peer-reviewed journal which covers all aspects of theoretical and practical research of materials science: synthesis, analysis of properties, technologies of materials processing and their use in modern manufacturing.

"Advanced Materials Research" is one of the largest periodicals in the field of materials engineering.

"Advanced Materials Research" specializes in the publication of thematically complete volumes from international conference proceedings and complete special topic volumes as well as stand-alone papers by individual authors.

Authors retain the right to publish an extended and significantly updated version in another periodical.

All published materials are archived with PORTICO and CLOCKSS.

Table of Contents

Editorial Note

Chapter 1: Advanced and Composite Materials

Atomic Layer Deposition of Inverse Opals for Solar Cell Applications
S.K. Karuturi, L.J. Liu, L.T. Su, W.B. Niu and A.L.Y. Tok 3

The Influence of Various Percentage of Al_2O_3 by Using Vortex Method to Tensile Strength and the Distribution of Al_2O_{3p} Composite
S. Junus, A. Zulfia, E. Tanoto and L. Mariani 8

Modifications of Multi-Walled Carbon Nanotubes on Zinc Oxide Nanostructures for Carbon Monoxide (CO) Gas Sensitive Layer
M. Iqbal, B. Yuliarto and N. Nugraha 12

An Investigation of Structure and Complex Impedance Behavior of Composite (1-*X*)$BA_{0.5}SR_{0.5}FE_{11.7}MN_{0.15}TI_{0.15}$ /*X*$LA_{0.7}BA_{0.3}MNO_3$
V.V.R. Repi and A. Manaf 16

Electrochemical Behavior of $Li_4Ti_5O_{12}$ under *In Situ* Process of Sintering and Surface Coating with Cassava Powder
B. Prihandoko, A. Subhan and S. Priyono 21

Synthesis of Highly-Ordered TiO_2 through CO_2 Supercritical Extraction for Dye-Sensitized Solar Cell Application
B. Priyono, A.H. Yuwono, B. Munir, A. Rahman, A. Maulana and H. Abimanyu 28

Deformation Behaviour of Silicon Carbide Reinforced Al-7Si Composite after Balistic Impacts
B.T. Sofyan, D. Rahmalina, B. Suharno and E.S. Siradj 33

Hydrogen Absorpsivity-Desorbsivity of Mg Doped by Ni, Cu, Al Produced by Mechanical Alloying
W. Widyastuti, B.P. Febrian and S. Sutarsis 37

Crystallite Growth Kinetics of $BaFe_{12}O_{19}$/$SrTiO_3$ Based Composites Derived from Mechanical Alloying
R.D. Widodo, A. Manaf and P. Sardjono 42

Crystal Structures and Thermal Properties of Bamboo Nanofiber Reinforced-Composite Friction Materials of Glass and Metal Wastes
S. Madnasri, S.S. Edi and D.S. Saputra 49

Formation and Characterization of MMCs Alloy Al-5%Cu-4%Mg/SiC(p) by Thixoforming Process
Y. Afandi, A. Zulfia, D. Priadi and I.N. Jujur 56

Study on PbSn Composites Produced by Powder Metallurgy as Core Bullet Projectile
W. Widyastuti, V.A. Setyowati and T. Akbar 60

Electroless Plating of Al_2O_3 Particles Reinforced Composites
A. Zulfia and A.I. Adyatma 66

$SrTiO_3$ Thin Films Deposition Using Pulsed Laser Deposition Technique
P. Dinari, C. Chandra, J. Suwardy, S. Mustofa and Y. Darma 72

Crystallite Size Characterization of Mechanically Alloyed of (Ba,Sr) Hexaferrite and (Ba,Sr) Titanate Composite System
N. Novizal, A. Manaf and P. Sardjono 76

New Technique for Conceptual Selection of Manufacturing Process and Material, Case Study: Metal Matrix Composite Component
N. Fatchurrohman, S. Sulaiman, S.M. Sapuan, M.K.A. Ariffin and B.T.H.T. Baharuddin 82

Nanosize Effects on Magnetic Properties and Peak Shifting of X-Ray Diffraction Pattern of $BaFe_{12}O_{19}$ Produced by Sol Gel Method
D. Suastiyanti, B. Soegijono and M. Hikam 87

Quasi-Solid State DSSC Performance Enhancement by Bilayer Mesoporous TiO_2 Structure Modification
R.A. Wahyuono and D.D. Risanti 93

Microstructure and Phase Analysis of $La_{0.8}Ba_{0.2}Ti_xMn_{(1-x)}O_3$ System for Microwave Absorber Material (x = 0 – 0.7)
W.A. Adi and A. Manaf 97

Crystallographic Properties of Aluminum-Doped Barium Zirconium Titanate Thin Films by Sol Gel Process
R. Andika and M. Hikam 101

Lead-Free Oxide Thin Films for Gas Detection
D. Fasquelle, S. Députier, M. Mascot, N. Uschanoff, V. Bouquet, V. Demange, M. Guilloux-Viry and J.C. Carru 105

Fabrication of Polymer Solar Cells on Flexible Substrate
E.S. Rosa and S. Shobih 112

Magnetic Behaviors of $BaTiO_3$-$BaFe_{12}O_{19}$ Nanocomposite Prepared by Sol-Gel Process Based on Differences in Volume Fraction
D. Suastiyanti, B. Soegijono and M. Hikam 118

Synthesis of Mesoporous Silica from Tetraethylorthosilicate by Using Sodium Ricinoleic as a Template and 3-Aminopropyltrimethoxysilane as Co-Structure Directing Agent with Volume Variation of Hydrochloric Acid 0.1 M
A. Andriayani, S.B. Sembiring, N. Aksara and N. Sofyan 124

Optimizing the Nanostructural Characteristics of Chemical Bath Deposition Derived ZnO Nanorods by Post-Hydrothermal Treatments
A.H. Yuwono, A. Sholehah, S. Harjanto, D. Dhaneswara and F. Maulidiah 132

Effect of CaO Dopant on the Dielectric Properties of NiO
S.A.S. Salim, J.J. Mohamed and Z.A. Ahmad 138

Numerical Modeling of Ship Composite-Based on Aluminum Casting as Alternative Materials for Ship Building
P.H. Tjahjanti, D. Manfaat, E. Panunggal, D. Darminto and W.H. Nugroho 143

High Coverage ZnO Nanorods on ITO Substrates via Modified Chemical Bath Deposition (CBD) Method at Low Temperature
A. Sholehah, A.H. Yuwono, N.R. Poespawati, A. Trenggono and F. Maulidiah 151

Quantum Approximation for Josephson's Tunneling in Th_x DUO_2 Nano Material for 535 Tesla at Muon Cyclotron
M. Hardiyanto 157

Microstructural Characterisation and Microwave Absorption Characteristics of $La_{(1-x)}Ba_xFe_{0.25}Mn_{0.5}Ti_{0.25}O_3$ (x = 0, 0.25, 0.75, 1)
E. Pratitajati and A. Manaf 161

Performance of Natural Carotenoids from *Musa aromatica* and *Citrus medic*a var Lemon as Photosensitizers for Dye-Sensitized Solar Cells with TiO_2 Nanoparticle
C.P. Eka, B. Yuliarto and S. Suyatman 167

Synthesis and Characterization of Nanocrystalline TiO_2 by Non-Aqueous Sol-Gel in Acidic Condition for Dye-Sensitized Solar Cells
L. Muliani and B. Sunendar 171

Removal of Heavy Metals from Aqueous Solution by Hydroxyapatite/Chitosan Composite
E. Kusrini, N. Sofyan, D.M. Nurjaya, S. Santoso and D. Tristantini 176

Photocatalytic Degradation of C.I. Reactive Red 2 by Using TiO_2-Coated PET Plastic under Solar Irradiation
T.E. Agustina, F.S. Arsyad and M. Abdullah 180

Synthesis of SnO_2 Nanostructure Thin Film and its Prospective as Gas Sensors
B. Yuliarto, N. Nugraha, B. Epindonta, R. Aditia and M. Iqbal 189

Preliminary Observation on Macro Texture of Nb_3Sn Low Temperature Superconductor (LTS)
A.W. Pramono 193

Characteristics of Heat Treated Al7Si-Mg-Zn - 5 wt.% SiC Squeeze Casted Composite with Variation of Mg Content for Tactical Vehicle Application
S.R. Sigit and B.T. Sofyan 198

Reduction of Nickel Ion Release on a TiO_2 Coated onto an Orthodontic Wire
S. Pintowantoro and Y. Setiyorini 204

Properties of Fe-Mn-C Alloy as Degradable Biomaterials Candidate for Coronary Stent
S. Harjanto, Y. Pratesa, Y. Prasetyo, B. Suharno, J. Syarif and F. Hakim 210

Synthesis and Characterization of Silica-Lavender Microencapsulation by Sol Gel-Emulsion Method for Anti Mosquito Textile
W.E. Mulyani and B. Sunendar 215

Sensitive Layer Thickness Dependence on Microcantilever Sensor Sensitivity
L. Aprilia, R. Nuryadi and D. Hartanto 219

Biocompatibility Improvement of NiTi Orthodontic Wire from Various Coatings
Y. Setiyorini and S. Pintowantoro 225

Synthesis and Characterization of Bacterial Cellulose-Based Carbon Nanotube by Catalytic Graphitization
E.R. Chaldun, M. Karina and B.S. Purwasasmita 232

Synthesis and Characterization of TiO_2 Nanoparticle Using Starch as a Template by Sol-Gel Method for the Application of UV Protection
M. Komalasari and B. Sunendar 237

Building Materials Composition Influence to Sound Transmission Loss (STL) Reduction
E. Setyowati and A.F. Sadwikasari 242

Contribution of Short Coconut Fiber to Pavement Skid Resistance
S.P. Hadiwardoyo, R.J. Sumabrata and P. Jayanti 248

Chapter 2: Polymer and Ceramics

Classification of Ceramic Tiles by Identifying Defect on Ceramic Tile Surface Using Local Texture Feature
B. Bertalya, P. Prihandoko, R. Oktavina and Y. Febrianto 257

Structural Characterization of Mullite-Based Ceramic Material from Al_2O_3 and Silica Xerogel Converted from Sago Waste Ash
H. Aripin, S. Mitsudo, E.S. Prima, I.N. Sudiana, H. Kikuchi, S. Sano and S. Sabchevski 262

Correlation of Normal Incidence Sound Absorption Coefficient (NAC) and Random Incidence Sound Absorption Coefficient (RAC) of Polyester/Ramie Fibre Composite Materials
M. Farid and T. Heriyanto 269

A Study on the Structure of Novel Polyurethanes Derived from γ-Valerolactone-Based Diol Precursors
M. Chalid, H.J. Heeres and A.A. Broekhuis 274

Grain Growth in Millimeter Wave Sintered Alumina Ceramics
S. Mitsudo, S. Inagaki, I.N. Sudiana and K. Kuwayama 279

The Dinamic Cyclic Trend Phenomena of Cement-Fly Ash Smart Concrete Compressive Strength and Resistivity in Various Composition of Polymer Carbon Fiber
Y. Lestari, S. Hardono, G. Ramadhan, A.Y. Akbar and E. Sugiarti 283

Preparation of the Edible Biocomposite Film Gelatin/Bacterial Cellulose Microcrystal (BCMC): Variation of Matrix Concentration, Filler, and Sonication Time
H. Hermansyah, R. Carissa, F. Anisa, M.P. Septa, T.S. Utami and R. Arbianti 287

Synthesis of Poly(1-vinyl-1,2,4-triazole) and Preparation of Proton Conducting Membrane for High Temperature Operation
G. Irfan, U.C. Sevim and A. Bozkurt 294

Characteristics of Environmental Friendly Labeled Plastic Shopping Bags in Indonesia
M. Cornelia, R. Syarief, H. Effendi and B. Nurtama 300

Chapter 3: Materials and Manufacturing Processes

SKD 61 Material Surface Treatment with Electric Discharge Machining Using Cu, CuCr & Graphite Electrodes and Dielectric Fluid Jatrophacurcas
T. Triyono, D. Priadi, E.S. Siradj and W. Winarto 307

Application of Shot Peening and Shot Blasting to Increase Hardness and Depth of Nitride Hardened Layer to the Modified H13 Steel as Die Casting Die Materials
M. Ariati and R. Aldila 313

Optimization of Multiple Performance Characteristics in the Wire EDM Process of AISI D2 Tool Steel Using Taguchi and Fuzzy Logic

Characterization of Al-7Si-Mg-Cu Turbine Impeller Produced by Investment Casting
M. Syahid, B.T. Sofyan, S.G. Basuki and B. Adam 324

Research on the Manufacturing of Steam Turbine Blade by Using Investment Casting Technology
Hafid 330

Mechanical Properties and Microstructure of Welded Dissimilar Metals Using Buttering & Non-Buttering Layer
W. Winarto, M. Anis and T.P. Hertanto 341

Comparison of Commercially Pure Titanium Surface Hardness Improvement by Plasma Nitrocarburizing and Ion Implantation
A.S. Darmawan, W.A. Siswanto and T. Sujitno 347

Effect of Phenolic Resin and Alignment to the Quality of Prototype Composite Railway Brake Blocks
A. Triono, W.P. Ign, S.S. Brodjonegoro and A. Ramelan 352

Effects of Welding Parameters in Micro Friction Stir Lap Welding of Aluminum A1100
A.S. Baskoro, A.A.D. Nugroho, D. Rahayu, Suwarsono, G. Kiswanto and W. Winarto 356

Preparation of Uranium Nitride from Uranium Metal through by Hydriding and Nitriding Process
H. Suwarno 360

Simulation of Metal Flow to Investigate the Application of Antilock Brake Mechanic System in Deep Drawing Process of Cup
S. Candra, I.M.L. Batan, A.S. Pramono and B. Pramujati 367

Effect of Equal Channel Angular Pressing and Post Heating on Microstructure and Hardness of Cu-Zn 70/30
S. Suryadi, R.A.M. Napitupulu, D. Priadi, A. Suhadi and E.S. Siradj 373

Materials Selection in Appropriate Technology Four Focuses in Design Thinking
C.P.M. Sianipar, H. Taufiq, H.R. Estiningtyas, K. Dowaki, A. Adhiutama and G. Yudoko 379

Study about Surface Hardening on Local Disc Brakes with Direct Current Plasma Nitrocarburizing Apparatus
U. Sudjadi 383

The Effect of Vertical Step Block Casting to Microstructure and Mechanical Properties in Producing Thin Wall Ductile Iron
R.D. Sulamet-Ariobimo, J.W. Soedarsono and I.P. Nanda 387

Resolving Individual Solute Levels of AA6061 through Multiple Sub-Ambient Temperatures Thermoelectric Power Measurements
D.D. Risanti and S. van der Zwaag 394

Effect of Rolling Direction to the Strength of a Thin-Walled Steel SHS Beam under Concentrated-Compressive Load and Bending Moment
A.M. Kadir, D. Priadi, E.S. Siradj and H. Setiyono 398

Optimization Design of Airfoil Propellers of Modified NACA 4415 Using Computational Fluids Dynamics
Sudarsono, Purwanto and J. Wahyuadi 403

Analysis of Micro-Channels Manufacturing of Acrylic Using Low Power CO_2 Laser
A.S. Baskoro, A. Siswanta and K.G.S. Ismail 408

Thickness and Fiber Content Optimization in VARTM Method for High Speed Craft
S. Sunaryo, G.L. Putra and S.M. Lestari 412

Vane-Turbine as an Energy Conversion in the Propeller Slipstream of Single Screw Ship
S. Leksono, I. Utama, M. Djoni and W.D. Aryawan 417

Application of Al_2O_3 Nanofluid on Sintered Copper-Powder Vapor Chamber for Electronic Cooling
N. Putra, W.N. Septiadi, R. Sahmura and C.T. Anggara 423

Real-Time Monitoring System of Dieless Bellows Forming Using Machine Vision
S. Supriadi, T. Furushima and K. Manabe 429

Springback Prediction Compensation and Optimization for Front Side Member in Sheet Metal Forming Using FEM Simulation
A.D. Anggono, W.A. Siswanto and B. Omar 436

Low Speed Electric Machine Used for Electric Generating from Savonius Windmill
Y.B. Lukiyanto 443

Physics and Chemistry Test on Aluminum-Based Composite Materials as an Alternative Material for the Manufacture of Brake Drum
P.H. Tjahjanti, W.H. Nugroho and H.C. Wahyuni 449

Oxidation Characteristics of Various Nickel Composite Coated on Ferritic Stainless Steel
A.R. Setiawan, R.D. Ramdan, B. Prawara, S. Steven and R. Suratman 455

Chapter 4: Corrosion and Degradation of Materials

Hot Corrosion of Aluminized 1020 Steel with NaCl Deposit
M. Badaruddin and S. Sugiyanto 463

Improvement of Stress Corrosion Resistance in Aluminum Alloy 7075 through Retrogression and Re-Aging Modification
E. Nurlia and S. Purwadaria 467

Behavior of CO_2 Corrosion of API 5L X52 Steel in NaCl Solution under Turbulent Flow Condition
A. Rustandi, N. Adhika, T. Prima and N. Aziz 476

Effectiveness of *Myrmecodia* Pendans Extract as Eco-Friendly Corrosion Inhibitor for Material API 5L Grade B in 3,5% NaCl Solution
A. Pradityana, S. Sulistijono and A. Shahab 484

Influence of Intermetallic Inclusion to Brittle Fracture of Electric Motor Shaft AISI 1045 under Torsion Loading
S. Suryadi, A.I. Karayan, A.C. Nugraha and B. Munir 492

High Temperature Oxidation Behavior of Co-Based Coating at 800^{o} C as Alternative Coating Material for SOFC Interconnect
A.R. Setiawan and R. Suratman 498

Contribution of Galvanizing Layer to Hydrogen Induced Cracking Failure of AISI 4140 Bolt for Padeye Fixing in Marine Environment
B. Munir, Suryadi and B. Suryo 502

Corrosion Inhibitor Performance with Presence of $FeCO_3$ Film in CO_2 Corrosion Environment under Fluid Flow Effect
S.M. Yaakob and M.C. Ismail 507

Corrosion of Concrete Using Portland Composite Cement and Rice Husk Ash under Simulated Acid Rain Environment
I.A. Ahmad, H. Parung, M.W. Tjaronge and R. Djamaluddin 511

Chapter 5: Extraction of Materials

The Influence of Coal and Reduction Process Parameters in Producing Iron Nugget
J.W. Soedarsono, A. Kawigraha, R.D. Sulamet-Ariobimo, M.A. Asy'ari, A. Yosi and E.M. Putra 517

Sulfuric Acid Leaching of Bangka Indonesia Ilmenite Ore and Ilmenite Decomposed by NaOH
L.H. Lalasari, R. Subagja, A.H. Yuwono, F. Firdiyono, S. Harjanto and B. Suharno 522

Submerged Ultrafiltration for Minimizing Energy Process of Refinery Wastewater Treatment
E. Yuliawati and A.F. Ismail 531

Anatase TiO_2 Enrichment from Bangka Ilmenite ($FeTiO_3$) and its Photocatalytic Test on Degradation of Congo Red
S. Sariman, Y.K. Krisnandi and B. Setiawan 538

Practical Isolation of Bullatacin from *Annona muricata* Leaves Extract Using an Open Column Chromatography Technique
K. Mulia, S.W. Winarcahyo, E. Krisanti and D. Kurniasuci 545

The effect of vertical step block casting to microstructure and mechanical properties in producing thin wall ductile iron

by A B

Submission date: 28-Aug-2020 03:49PM (UTC+0800)
Submission ID: 1375373758
File name: nd_mechanical_properties_in_producing_thin_wall_ductile_iron.pdf (1.38M)
Word count: 3733
Character count: 18313

Advanced Materials Research Vol. 789 (2013) pp 387-393 *Online: 2013-09-04*
© (2013) Trans Tech Publications, Switzerland
doi:10.4028/www.scientific.net/AMR.789.387

The Effect of Vertical Step Block Casting to Microstructure and Mechanical Properties in Producing Thin Wall Ductile Iron

Rianti Dewi Sulamet-Ariobimo[1,a], Johny Wahyuadi Soedarsono[2,3,b], and Is Prima Nanda[4]

[1] Mechanical Engineering Department, Faculty of Industrial Technology, Universitas Trisakti, Jakarta, Indonesia
[2] Department of Metallurgy and Materials, Faculty of Engineering, Universitas Indonesia, Depok, Indonesia.
[3] Politeknik Negeri Jakarta, Depok, Indonesia.
[4] Department of Mechanical Engineering, Faculty of Engineering, Universitas Andalas, Padang, Indonesia.
[a] riantiariobimo@yahoo.com , [b]jwsono@metal.ui.ac.id

Keywords: casting design; TWDI; vertical step block; Y-block principle; pouring basin position

Abstract

Thin wall ductile iron (TWDI) is introduced to fulfill the needs of lighter material in automotive parts that will reduce fuel consumption. Problem occurs during the production of TWDI due to the casting thickness. TWDI casting thickness classified to below 5 mm. Many designs have been made to answer the problem in producing thin wall ductile iron. Soedarsono et al established vertical step block casting design. This design based on Y-block principle that allows direct pouring of liquid metal to the mold without passing any gating system. This design will increase casting yield. The parameter of this research is pouring basin placement to study the effect of plate arrangement to filling and solidification. This research is conducted to see the effect of pouring basin placement to microstructure and mechanical properties of TWDI. The Design is made to produce 5 plates with different thickness that is 1, 2, 3, 4, and 5 mm. All of the plates arranged parallel in line. Pouring basin located in 2 ways. The first type located pouring basin above the plate of 5 mm thickness while the second one located it above the plate with 1 mm thickness. The first type coded as T4 while the second coded as T5. The moulds made from furan sand. The result shows although cold shut occurred in both pouring basin placements due to pouring discontinuity but shrinkage only formed in T5 on its plate with 1 mm thickness. Microstructure of all the plates presented nodule graphite in pearlite matrix. Carbide and skin effects also detected. Average nodularity is above 80% while the nodule count is between 614 to 1269 nodule/mm^2. Most of the Brinell hardness number exceeded maximum limit given by JIS G5502 but the UTS is below the minimum limit except for 3 mm plate thickness of T5. All elongation values below the minimum standard. The results confirm that pouring basin location is important in casting design following Y-Block principle.

Introduction

Energy crisis has force human kind to change the way they consume it. Lighter materials are applied to machine components to reduce the energy consumption during the operation. Since reducing 100 kg of car's weight will reduce 0.5 liter of fuel for 100 km [1]. Unfortunately, light materials such as aluminum consume a lot of energy during their production. Thin wall ductile iron (TWDI) is developed to combine superior ability owns by ductile iron with lightweight characteristic. Apart from that TWDI is energy friendly during the production. These combinations will form a material with the ability to fulfill the needs. The main problem in the producing TWDI is the cooling rate; since the thickness of TWDI is classified to be below 5 mm. [2-5].

Researches take casting design to deal with TWDI cooling rate since casting design is a free parameter. Changing in casting design will not disturb material supplies, equipments, and process that have been established. Javaid et al. [6] used a step block casting design while Showman et al [7] introduced modified and horizontal groove step block casting designs and Pedersen et al used

stepped block with feeder [8]. Beside the step block designs specific casting designs also introduced in producing TWDI. Stefanescu and his research group [4,9] have used special horizontal and vertical gating designs. Followed by Schrems et al. [1] who created horizontal casting design, INTEMA group developed special horizontal and vertical gating system [2,3,13]. In addition, Labrecque and his associates [10-12] created their own casting design as well as

Soedarsono et al [5,14-19] together with his colleagues developed several special vertical casting designs which can be classified into 2 groups. In the first group, the designs were developed from Stefanescu et al vertical casting design [3]. Soedarsono et al modified the gating system designs purposed by Stefanescu et al with three variations, that are: the bottom gating, the bottom gating with supporting gates, and the top gating gravity [5,14-19]. While in the other groups Soedarsono et al applied the Y-block principle, which can improve the casting yield. Y-block principal is a casting method without using gating system. Soedarsono et al introduced a new concept of plate arrangement based on its thickness, which contradicted the general principle of casting. This concept puts the thinnest plate near to ingate. The result of both the simulation and the experiment emphasizes that there was no trace of premature solidification, the filling process was successful, and all the plates were fully cast. [5,14-19].

This paper discusses the effect of Y-block principle casting design to microstructure and mechanical properties in producing TWDI plates.

Experiment Methods

Casting designs used in this work is represented by Figure 1. Two designs were built and coded as T4 and T5. The dimension of the plates is 75 X 150 mm with the thicknesses of 1, 2, 3, 4, and 5 mm. Every mould produces five plates. The plates are arranged in sequences. In T4 the pouring basin was put directly above the plate with 5 mm thickness while in T5 the pouring basin was placed above 1 mm thick plate.

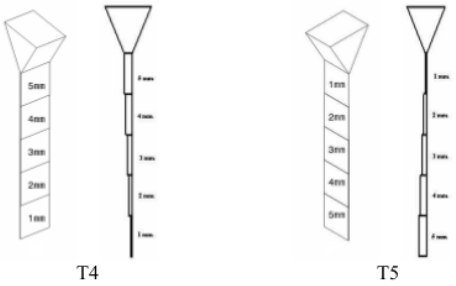

Figure 1. Casting Design

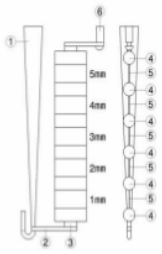

Figure 2. Casting Design of P1T1 [4,14-19]

The work was done in both simulation and experiment. Simulation on casting designs used Z-Cast program version 2.5. It ran for flow, solidification, and shrinkage analysis. Z-Cast is casting process simulation system developed by KITECH for over 20 years and fully verified at real manufacturing fields for various casting processes. The simulation was made base on assumptions that the process will be held in equilibrium condition since the molten metal used is ductile iron. The solidification process was assumed as alloyed solidification process with phases changing. The heat transfer dominant in the process will be convection ($\partial T/\partial x$) and every calculation were made base on it [18].

The experiment was done on the foundry scale and the moulds were made from furan sand. The metal cast was Ferro Casting Ductile (FCD) within the grade of 450 (JIS 2000). There was a chemical composition examined before conducting the liquid treatment process. The liquid treatment used was 12 kg Fe-Si-Mg with 6%Mg as the nodularising agent in the sandwich method with a tapping temperature of 1500^{O}C. Inoculants were also placed in the ladle. The inoculant used in this research was S70 with the composition of 1.5%Ca; 72.95%Si; 0.86%Al; 2.1%Ba. Pouring

temperatures were 1450^{O}C and 1445^{O}C. The observations made included carbides appearance, nodule count, nodularity and nodule diameter uniformity. The calculations of nodular graphite characteristics were made by using manual calculation based on American Standard Testing Material (ASTM) A427 and also by using Cyuuzou Kun. Cyuuzou Kun is an imagine analyses software used in Iwate University.

Discussion

The chemical compositions of molten metal shows by Table 1 are all in range. There are some differences but the differences are not significant. Chemical composition of the molten metal fulfilled the requirements of FCD450.

Table 1. Chemical Composition – weight, [%].

Element/Pouring	C	Si	Mn	P	S	Cu	Ni	Cr	Mg
P1	3.8	2.6	0.37	0.02	0.02	0.04	0.03	0.04	0.04

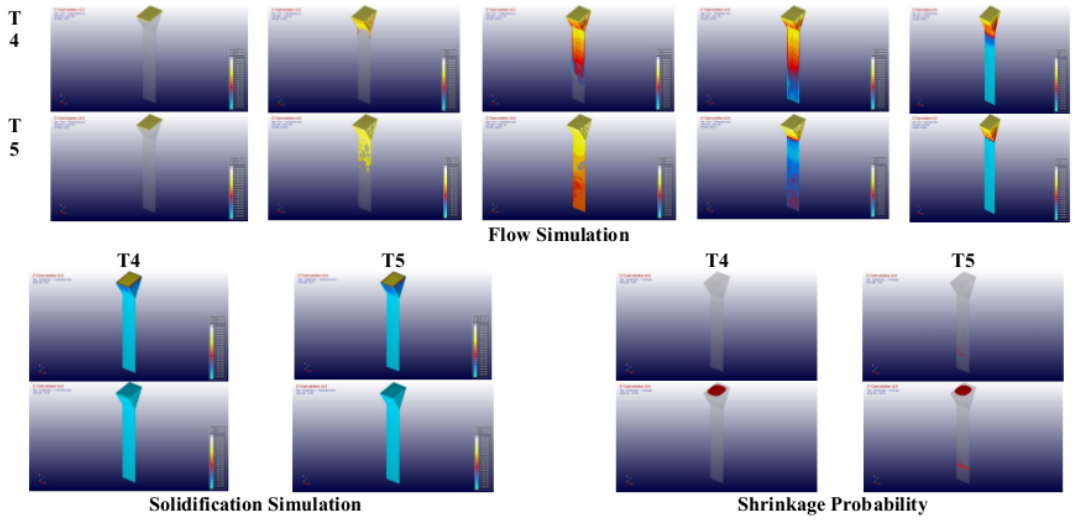

Figure 3. Simulation Result of T4 and T5

Simulations of both designs present different flow patterns (Fig. 3). Mould filling process is faster in T5 (0.75 s) than T4 (1.25 s). Filling process in T4 begins from both side of mould opening. Molten metal fills the mould with left and right side flows. The molten metal stream is smooth and still. Small turbulence occurs and temperature drops happens but localize when the mould full. The filling pattern in T4 is one direction flow. As for T5, the molten metal enters the mould through the whole opening with heavy stream. Heavy turbulence happens and the filling pattern is two ways direction. Although temperatures gradation missing when the mould full but during the filling heavy temperature gradation happens in several areas. This might cause different development of microstructure.

Results of solidification simulation (Fig. 3) show same pattern for T4 and T5. All plates already have blue color in the beginning of the simulation. When simulated the solidification only happens in pouring basin with the same pattern for both designs. Results of shrinkage (Fig. 3) presents different pattern for T4 and T5. In T4, shrinkage forms in the pouring basin area. This will do no harm to the cast plates. While in T5, shrinkage also forms in the bottom of 4 mm plate thickness.

During pouring process, discontinuity happens. This might cause defects in macro or micro condition. Both T4 and T5 show cold shut defects (Fig. 4) but discontinuity effects T5 more than T4. Beside cold shut, shrinkage also forms in T5. This is happen because T5 has smaller opening,

which acts as an ingate. Simulation of T5 has predicted the formation of shrinkages and shrinkages do formed in the cast but the positions are not the same. Analysis result of shrinkages in T5 show that the shrinkages form due to discontinuity of molten metal during pouring.

T4 T5

Figure 4. Casting Result of T4 and T5

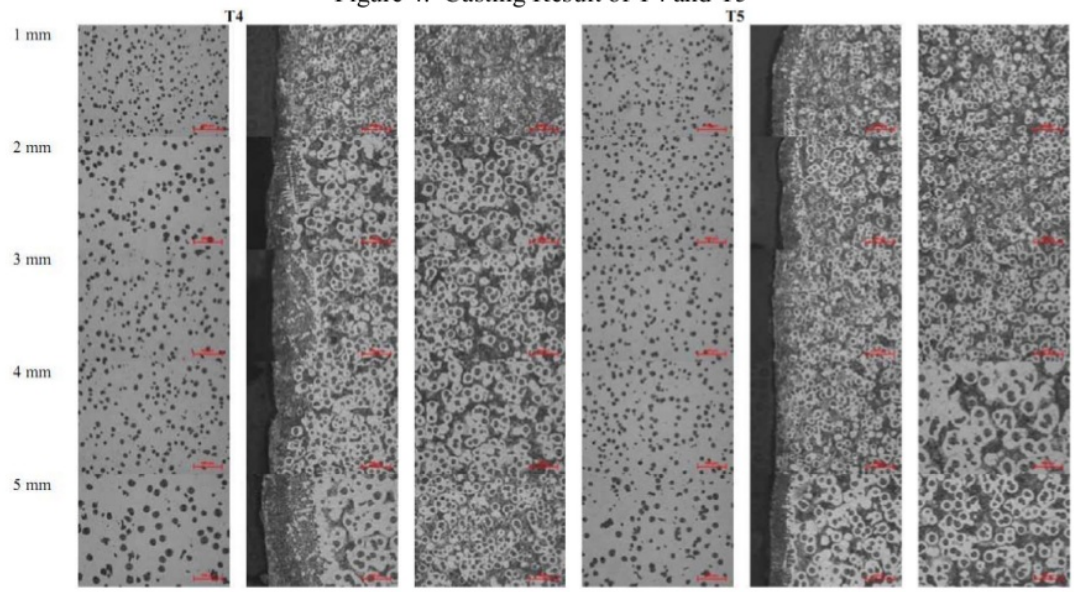

Figure 5 Microstructure of T4 and T5

Metalographic examinations of non-etched microstructures show same result for T4 and T5 that is nodule graphite (Fig. 5). Defects form in T5 and seen clearly in 3 mm plate thickness. Qualitatively, nodule graphite in T5 is smaller than T4. The nodule graphite of T5 appears to be similar in all thickness and distributes evenly except for plate with 5 mm thickness. This proves that temperature gradation (Fig. 3) happened during the filling process do not affects the final result. The nodule graphite in T4 look bigger in plate thickness of 2 mm and 5 mm look bigger compared to the other plates. T4 seems to have higher nodularity than T5. The etched microstructures show that the matrix is pearlite for both designs. Carbides also form in both designs and so do skin effects. Heavy carbide is show by plates with the thickness of 1, 3, 4 mm for T4 and 1, 2 mm for T5. The pearlite composition looks decrease as the thickness of the plate increase. In plate with 5 mm thickness, the matrix becomes pearlite/ferrite. A same thing happens to carbide. The composition of carbide seems to decrease as the thickness of the plate increase. Skin effects do not form in all plates. Plate with the thickness of 1 mm in T4 and 4 mm in T5 do not show any presence of skin effects. The qualitative analysis of microstructure confirms the simulation result. Simulation shows that T5 does not have temperature degradation when the filling process finished while T4 has localized one. This situation suspects to be the caused of nodule graphite condition. The designs of T4 and T5 give different matrix compared to previous research done by Soedarsono et al using the design of T1 (Fig. 2). The microstructure resulting from T1 for both plate arrangements (P1T1 and P2T1) is nodule graphite in ferrite matrix [19].

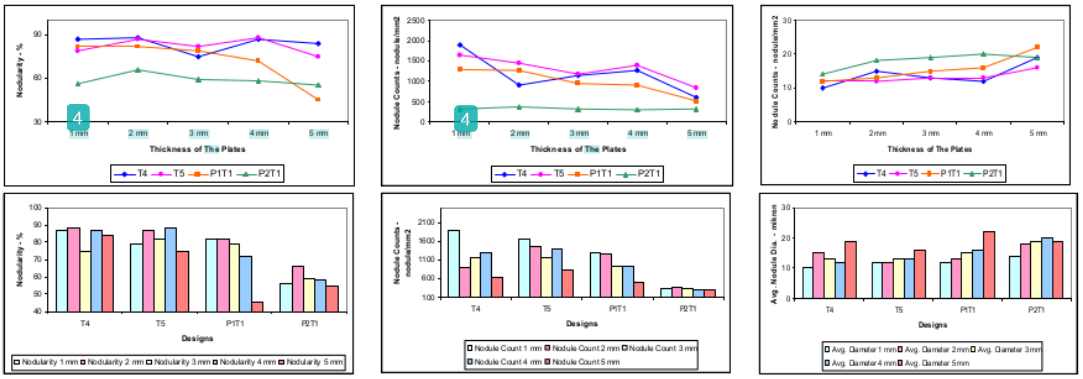

a. Nodularity b. Nodule Counts c. Average Nodule Diameter

Figure 6 The Characteristic of Nodule Graphite for T4, T5, P1T1 [19] and P2T1 [19]

Quantitative examination of nodule graphite presents average nodularity of T4 is 84% while T5 is 82%. This confirmed that T4 has higher nodularity than T5. Nodularity of T4 is between 75 to 88%, while T5 are between 75 to 88%. Nodularity in T4 plates is distribute evenly more than T5. The trend of nodularity for T4 and T5 do not show any similarity if compares to P1T1 and P2T1. Averages nodularity gain by T4 and T5 are higher than P1T1 and P2T1, even when the nodularity of plate with 5 mm thickness from P1T1 excluded.

Average nodule counts show that T5 (1302 nodule/mm^2) has higher nodule count than T4 (378 nodule/mm^2). Range of T4 nodule counts are from 614 to 1898 nodule/mm^2. While in T5, the nodule counts are from 840 to 1649 nodule/mm^2. This confirmed the qualitative examination made previously. Nodule counts in T5 plates show more similarity than T4. The difference between the highest and the smallest nodule count from plates in T5 is 49% while in T4 is 68%. T5 has higher nodule count compares to P1T1 and P2T1 [19]. Although nodule count in P2T1 is the lowest among others but the similarity of nodule count between plates in P2T1 is the highest. T5 has the smallest average nodule diameter (13.2 micron). This finding confirms T5 as the highest in nodule counts.

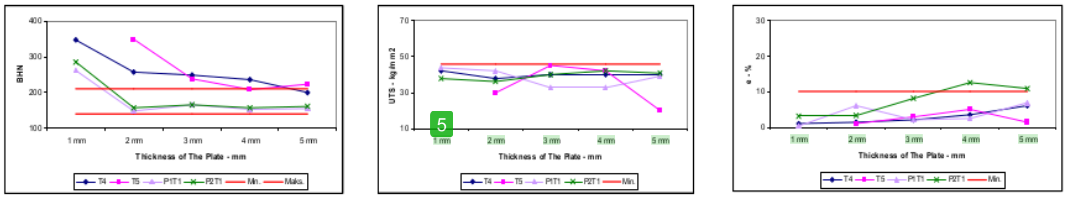

a. Brinell Hardness Number b. Ultimate Tensile Strength – UTS c. elongation – e

Figure 7 Mechanical Properties of T4, T5, P1T1 [19] and P2T1 [19]

Almost all of Brinell Hardness Number (BHN) of T4 and T5 exceeded the maximum limit of FCD450 (Fig. 7). This is happen because the presence of carbide and pearlite as the matrix. In T4 the BHN of plate with 5 mm thickness enters the standard of FCD450 because the matrix is pearlite/ferrite. While the BHN in T5 on its plate with 4 mm thickness close (0.5%) to the maximum limit because the composition of the matrix is all almost pearlite. Carbide is trace but very little. The BHN obtains by T4 and T5 confirmed the presence of carbide. When the BHN of T4 and T5 compare to P1T1 and P2T1, the BHN of P1T1 and P2T1 all are below maximum standard except for plate with 1 mm thickness. BHN of plates with 1 mm thickness from both designs also exceeded the maximum limit and carbide is present.

Ultimate tensile strength of T4 and T5 do not pass the minimum limit of FCD450, but T4 has higher and more even than T5. The smallest UTS achieve by plate produce in T4 design is 17% below the minimum limit. While for T5 is 57%. Based oh microstructures condition and analysis this failure suspects as the effect of defects that formed especially in on T5 where 2 kinds of defects are found. Same thing happens in elongation. The elongation of both T4 and T5 do not reach the minimum

limit. Elongation of T4 exhibits its general that is elongation will increase with the increase of thickness, but this phenomenon is not happens in T5. Average UTS of T4 (40 kg/mm^2) is higher compare to P1T1 (38 kg/mm^2) and P2T1 (39 kg/mm^2) [19]. Reverse condition is happen for elongation. The elongation of P1T1 and P2T1 [19] are higher compare to T4 and T5.

Conclusion

This work finds that the designs made by Soedarsono et al have able to produce TWDI plates with different kinds of matrix. The designs of vertical step block casting following Y-block principle produce TWDI with the microstructure of nodule graphite in pearlite matrix while the gating system designs produce TWDI with the matrix of ferrite.

When cooling rate is determined by the presence of microstructure then designs of vertical step block casting following Y-block principle has higher cooling rate compare to the designs developed from Stefanescu vertical casting design.

The quantitative microstructures analysis shows high nodularity and nodule count owned by all of the plates but their mechanical properties have not fulfill the standard of FCD450, this is caused by the presence of carbide and defects in the plates.

Temperature gradation during filling process will not affect the development of microstructures but the temperature condition when the mould fully fulfill will. Stream turbulences are not always detrimental to casting properties.

Experiment results to a certain limit confirmed simulation results. Full confirmation cannot be established due to discontinuity that happened during the pouring process.

The highest nodularity is 88% achieve by 2 mm plate thickness produces by T4 and 4 mm plate thickness produces by T5. The highest nodule count is 1898 nodule/mm^2 achieved by 1 mm plate thickness produce by T4. The smallest average nodule diameter is 10 micron achieved by 1 mm plate thickness produce by T4. The highest average nodularity is 84% achieved by T4 while the highest nodule count is 1302 nodule/mm^2 achieved by T5. The smallest average nodule diameter is 13.2 micron achieved by T5. Compared to P1T1 and P2T1 the nodularity of T4 is the highest while nodule count of T5 is the highest among others.

Almost all BHN of T4 and T5 exceeded maximum limit due to the presence of pearlite matrix and carbide. The highest BHN is 350 achieved by 2 mm plate thickness produces by T5, the smallest is 201 achieved by 5 mm plate thickness produces by T4. The highest UTS is 45 kg/mm^2 achieved by 3 mm plate thickness produces by T5, the smallest is 20 kg/mm^2 achieved by 5 mm plate thickness produces by T5. The highest elongation is 6% achieved by 5 mm plate thickness produces by T4, the smallest is 1% achieved by 1 mm plate thickness produces by T4 and 2 mm plate thickness produces by T5.

Acknowledgment

The authors wish to show their gratitude to The Secretary of National Education Republic Indonesia for the research grants and PT. Geteka Founindo for their foundry and castings.
The authors also wish to show their gratitude to Department of Metallurgy and Material Engineering Faculty Universitas Indonesia for Z-Cast Simulation Program and Iwate University for quantitative analysis of microstructure.

REFERENCE

[1] K. K Schrems, J. A. Hawk, Ö. N. Dogan and A. P. Druschitz, SAE Tech. Paper Doc. No. 2003-01-0828 (2003).
[2] M. Caldera, M. Chapetti, J.M. Massone, and J.A. Sikora: Mater. Sci. Technol, Vol. 23 No. 8 (2007), pp. 1000.
[3] R.A. Martinez, R.E. Boeri, and J. A. Sikora: Proceeding of 2002 world conference on ADI, AFS(2002).
[4] D.M. Stefanescu, L.P. Dix, R.E. Ruxanda, C. Corbitt-Coburn, and T.S. Piwonka: AFS Trans, Vol. 110 (2002), pp. 1149.

[5] J.W. Soedarsono and R. D Sulamet-Ariobimo: AMM, 415-417(2012), pp. 3301.
[6] A. Javaid, K. G. Davis, and M. Sahoo: *Mod. Cast.*, 90(2000), pp. 39.
[7] R. E. Showman, R. C. Aufderheiden and N. Yeomans: *Mod. Cast.*, 96(2006), pp. 29.
[8] K. M. Pedersen, N. S. Tiedjen: *Mater. Charact.*, 09(2007).
[9] L. P. Dix, R. Ruxanda, I. Torrance, M. Fukumoto, and D. M. Stefanescu: AFS Trans, Vol. 111 (2003), pp. 895.
[10] C. Labreque, M. Gagné, A. Javaid and M. Sahoo: *Int. J. Cast Metal Res.*, 16(2003), pp. 313.
[11] C. Labreque, M. Gagné, and A. Javaid: AFS Trans, Vol. 113 (2005), pp. 677.
[12] C. Labreque and M. Gagné: AFS Trans, Vol. 108 (2000), pp. 31.
[13] R.C. Aufderheide, R. E. Showman and M. A. Hysell: AFS, 113(2005), pp. 567.
[14] J.W. Soedarsono, B. Suharno and R. D Sulamet-Ariobimo: AMR, 415-417(2012), pp. 831-837
[15] J.W. Soedarsono, B. Suharno and R. D Sulamet-Ariobimo: AMM, 152-154(2012), pp. 1607.
[16] R. D. Sulamet-Ariobimo, J. W. Soedarsono and B. Suharno, "Effect of Casting Design to Microstructure and Mechanical Properties of 2 mm TWDI Plate" AMR, in press.
[17] R. D. Sulamet-Ariobimo, J. W. Soedarsono and B. Suharno: Solid State Phenomena, in press (2013).
[18] T.P. Soemardi, J.W. Soedarsono, and R.D. Sulamet-Ariobimo: International Symposium on Transport Phenomena, ISTP-22(2011).
[19] B. Suharno, J. W. Soedarsono, T. P. Soemardi, and R. D. Sulamet-Ariobimo: AMR, 277(2011), pp. 66.

Advances in Materials, Processing and Manufacturing
10.4028/www.scientific.net/AMR.789

The Effect of Vertical Step Block Casting to Microstructure and Mechanical Properties in Producing Thin Wall Ductile Iron
10.4028/www.scientific.net/AMR.789.387

DOI References
[2] M. Caldera, M. Chapetti, J.M. Massone, and J.A. Sikora: Mater. Sci. Technol, Vol. 23 No. 8 (2007), p.1000.
http://dx.doi.org/10.1179/174328407X185910

The effect of vertical step block casting to microstructure and mechanical properties in producing thin wall ductile iron

ORIGINALITY REPORT

5%	4%	5%	3%
SIMILARITY INDEX	INTERNET SOURCES	PUBLICATIONS	STUDENT PAPERS

PRIMARY SOURCES

1	www.micromechanics.cn Internet Source	2%
2	R.D. Sulamet-Ariobimo, M. Fadlan, S. Kamili, T. Sukarnoto, Y. Mujalis, Y. Oktaviano. "Effects of Austempering Process to Mechanical Properties of Thin Wall Ductile Iron Connecting Rod.", IOP Conference Series: Materials Science and Engineering, 2019 Publication	1%
3	www.ttp.net Internet Source	1%
4	www.orthomedical.de Internet Source	1%
5	tportho.com Internet Source	1%

Exclude quotes	On	Exclude matches	< 1%

Exclude bibliography On